HHS Public Access

Author manuscript

Luminescence. Author manuscript; available in PMC 2019 September 05.

Published in final edited form as:

Luminescence. 2018 November ; 33(7): 1194–1201. doi:10.1002/bio.3535.

Two colorimetric fluorescent turn-on chemosensors for detection of $Al^{3+}$and N_3^-: Synthesis, photophysical and computational studies

Fasil Abebe, **Treshaun Sutton**, **Pierce Perkins**, **Roosevelt Shaw**

Department of Chemistry, Morgan State University, Baltimore, MD, USA

Abstract

Two new rhodamine derivative L_1 and L_2 bearing 2-methoxy-1-naphthaldehyde and 5-bromo-3-methoxy salicylaldehyde units were designed and synthesized using microwave-assisted organic synthesis and utilized towards sequential fluorescence detection of aluminum ion (Al^{3+}) and azide (N_3^-) in aqueous acetonitrile solution. Aluminum ion (Al^{3+}) triggers the formation of highly fluorescent ring-open spirolactam. The fluorescence and colorimetric response of the L_1-Al^{3+} and L_2-Al^{3+} complexes were quenched by the addition of N_3^-, which extracting the Al^{3+} from the complexes and turn-off the sensors, confirming that the recognition process is reversible. The recognition ability of the sensors was investigated by fluorescence titration, Job's plot, ^{1}H-NMR spectroscopy and density functional theory (DFT) calculations.

Keywords

Al^{3+} and N_3^-; colorimetric; fluorescence; rhodamine

1 | INTRODUCTION

Aluminum is the most abundant metallic element in the earth and is found in its ionic form Al^{3+} in most animal and plant tissues and in natural waters because of acidic rain and human activities.[1] The wide-spread use of aluminum in pharmaceuticals, cooking utensils, aluminum foil, vessels, and trays results in moderate increase in Al^{3+} concentration in food. The iron binding protein is known to be the main carrier of Al^{3+} in plasma, and Al^{3+} can enter the brain and reach the placenta and fetus. In addition, Al^{3+} has been implicated as a causative factor of Alzheimer's disease and associated with damage to the central nervous system in humans.[2,3] The World Health Organization (WHO) listed Al^{3+} as one of the prime food pollutants and limited its concentration to 200 μg L^{-1} in drinking water.[4] WHO recommended tolerable weekly dietary human intake of Al^{3+} is 7.0 mg kg^{-1} body weight.[5] Due to the potential impact of Al^{3+} on the environment and human health, the effective detection of Al^{3+} ions is needed. Fluorescent chemosensor has been regarded as an effective

Correspondence: Fasil Abebe, Department of Chemistry, Morgan State University, Baltimore, MD 21251, USA., fasil.abebe@morgan.edu.

SUPPORTING INFORMATION

Additional supporting information may be found online in the Supporting Information section at the end of the article.

method for tracing relevant ions and shows its unique potential advantages. Unfortunately, the determination of Al^{3+} is complicated by its poor coordination ability, a strong tendency to hydration, and lack of suitable spectroscopic characteristics.[6] It is well known that Al^{3+} prefers a coordination sphere containing N and O as hard-base donor sites. Schiff bases are known to be good ligands which provide a hard-base environment for the hard-acid Al^{3+}. Most of the reported Al^{3+} sensors involve complicated synthetic routes with harsh reaction conditions and expensive chemicals.[7] Therefore, it is important to develop an easily synthesizable selective and sensitive chromo/fluorogenic dual signaling sensor for Al^{3+} in aqueous media.

In recent years the field of anion recognition has grown exponentially due to the significance of anions in environmental, biological and industrial systems.[8] Among several anions, azide ion (N_3^-) is equally important as they are widely used in automobile airbags, airplane escape chutes, pest control, agriculture, and laboratory research. It resembles carbon monoxide in its irreversible binding to heme cofactors and inhibits mitochondrial respiration causing impaired memory blocking the cytochrome c oxidase.[9,10] A number of chemosensors have appeared in the literature for either Al^{3+}[11] or N_3^- ions,[12] but sensors for both Al^{3+} and N_3^- ions are scarce. The few sensors for both ions suffer from a tedious synthesis procedure, low sensitivity or slow response, turn-off fluorescence response, poor water solubility, and interference from other ions.

Rhodamine-based compounds have been widely used as chemosensors due to their remarkable spectroscopic properties including high absorption coefficients, high fluorescent quantum yields, and excitation and emission with the visible wavelength region.[13] The non-fluorescent spirolactam of rhodamine derivatives can undergo a ring opening in the presence of metal ions to give the highly fluorescent form.[13,14] The ring-open form is pink in color with orange or sometimes green fluorescence.[15] The metal ion sensing behavior of these rhodamine-based optical sensors is very interesting. This is an excellent mechanism which we can use to detect metal ions and several rhodamine based sensors have been reported for ions.[16–23]

We are now able to report a newly designed and structurally characterized rhodamine Schiff base compounds L_1 and L_2 which are able to sense micromolar levels of Al^{3+} ions by chelation-enhanced fluorescence (CHEF) process, and Al^{3+} complexes L_1-Al^{3+} and L_2-Al^{3+} behave as highly selective chemosensors for N_3^- ions by quenching of the fluorescence in acetonitrile/water (CH_3CN/H_2O) medium at 25°C. The competitive ions do not affect the selectivity and specificity of the sensors in the detection of Al^{3+} and N_3^- ions. To the best of our knowledge, reports of Al^{3+} bound sensor for the detection of N_3^- ions are quite rare. In this work, we introduce a microwave-assisted organic synthesis (MAOS) method to synthesis L_1 and L_2 in a simple approach; the strategy is shown in Scheme 1.

2 | EXPERIMENTAL

2.1 | Chemicals and instruments

All the reagents and solvents were purchased as analytical-grade and used without further purification unless otherwise stated. The stock solutions of metal ions were prepared from

their nitrate and chloride salts and anion species from their tetrabutylammonium salts. Distilled deionized water was used throughout the experiments. ^{1}H-NMR and ^{13}C-NMR spectra were recorded using an Avance 400 MHz spectrometer (Bruker Billerica, Karlsruhe, Germany) with tetramethylsilane (TMS) as internal standard and deuterated chloroform ($CDCl_3$) as solvent. NMR spectra were analyzed using MestReNova software (version 10, Mestrela Research, Feliciano Barrera-Bajo, Spain). The IR spectrum was obtained using FT-IR spectrometer (Shimadzu, IRAffinity-1S, Columbia, MD, USA). High resolution electrospray ionization mass spectrometry (ESI-MS) was acquired with a Bruker Apex-Qe instrument. All UV-vis spectroscopy experiments were recorded using a Cary UV/vis spectrophotometer 5000 (Varian, Walnut Creek, CA, USA). Fluorescence emission spectra experiments were measured using a Cary 60 series spectrometer (Agilent, Walnut Creek, CA, USA), with excitation and emission slit widths of 5 nm and excitation wavelength at 510 nm. MAOS reactions were carried out in a single mode Biotage Initiator 2.0 (Biotage, Uppsala, Sweden).

2.2 | Microwave-assisted synthesis and characterization of L_1 and L_2

Sensors L_1 and L_2 were synthesized from the parent rhodamine B and aromatic aldehydes (2-methoxy-1-naphthaldehyde and 5-bromo-3-methoxy salicylaldehyde) in a two-step Schiff base condensation using MAOS heating protocols, as described in Scheme 1. Compound **2** was synthesized according to the reported procedure.[24]

2.2.1 | Synthesis of sensor L_1—Using microwave heating protocol: A mixture of compound **2** (105 mg, 0.230 mmol), 2-methoxy-1-naphthaldehyde (41 mg, 0.220 mmol) and ethanol (2 ml) was placed in a 10 ml reaction vial. The resulting mixture was stirred to make it homogeneous and it was placed in the cavity of a biotage microwave reactor. The closed reaction vessel was run under pressure and irradiated for 10 min at 100°C. After cooling to room temperature, the resulting solid was filtered and washed three times with cold ethanol. After drying, the ligand L_1 was isolated to give in 92% yield. Melting point: 244–246°C; ^{1}H-NMR ($CDCl_3$), δ (ppm):9.63 (1H, s, N=C-H); 8.77 (1H, d, *J* = 7.4 Hz, H-Ar), 7.74 (1H, d, *J* = 8.4 Hz, H-Ar), 7.71 (1H, d, *J* = 8.0 Hz, H-Ar), 7.63 (1H, d, *J* =7.7 Hz, H-Ar), 7.48–7.51 (2H, m, H-Ar), 7.15–7.27 (2H, m, H-Ar),7.12 (1H, d, *J* = 8.4 Hz), 7.09 (1H, d, *J* = 4.9 Hz), 6.63 (2H, d, *J* =8.8 Hz), 6.44 (2H, d, *J* = 2.2 Hz), 6.28 (2H, dd, *J* = 8.8 Hz, 2.6 Hz), 3.82 (3H, s, OCH_3), 3.31 (8H, q, *J* = 6.9 Hz, NCH_2CH_3), 1.14 (12H, t, *J* = 6.9 Hz, NCH_2CH_3). ^{13}C-NMR ($CDCl_3$), δ (ppm): 164.6, 157.8, 153.4, 151.7, 148.8, 147.6 (N=C-H), 137.6, 133.1, 131.9, 130.3, 129.2, 128.1, 127.0, 126.7, 124.0, 123.2, 116.8, 112.9, 108.1, 107.9, 106.5, 104.6, 79.9, 66.3 (spiro carbon), 56.7, 44.3 (NCH_2CH_3), 12.7(NCH_2CH_3); HRMS (ESI): *m/z* calcd for $C_{40}H_{40}N_4O_3$: 625.3173; Found: 625.3176 $[M + H]^+$.

2.2.2 | Synthesis of sensor L_2—Using microwave heating protocol: A mixture of compound **2** (100 mg, 0.220 mmol), 5-bromo-3-methoxy salicylaldehyde (51 mg, 0.221 mmol) and ethanol (2 ml) was placed in a 10 ml reaction vial. The resulting mixture was stirred to make it homogeneous and it was placed in the cavity of a biotage microwave reactor. The closed reaction vessel was run under pressure and irradiated for 10 min at 100°C. After cooling to room temperature, the resulting solid was filtered and washed three times with cold ethanol. After drying, the ligand L_2 was isolated to give in 88% yield. ^{1}H-

NMR ($CDCl_3$), δ (ppm):11.11 (1H, s, −OH), 8.94 (1H, s, −CH=N), 7.96 (1H, t, *J* = 6.6 Hz, −Ar), 7.49 (2H, m, −Ar), 6.86 (1H, d, *J* = 6.6 Hz, −Ar), 7.50 (2H, s, −Ar), 6.51–6.43 (4H, m, −Ar), 6.25 (2H, d, *J* = 7.5 Hz, −Ar), 3.82 (3H, s, $-OCH_3$), 3.31 (8H, q, NCH_2CH_3), 1.16 (12H, t, *J* = 6.6 Hz, NCH_2CH_3) ^{13}C-NMR ($CDCl_3$), δ (ppm): 163.6, 152.7, 148.5, 146.6 (−CH=N), 138.5, 138.1, 137.7, 134.0, 128.9, 128.5, 127.5, 123.1, 121.8, 121.3, 108.1, 108.0, 106.5, 104.8, 97.3, 80.9, 65.5 (spiro carbon), 56.1, 43.6 (NCH_2CH_3), 12.4 (NCH_2CH_3). HRMS (ESI): *m/z* calcd for $C_{36}H_{37}BrN_4O_4$: 669.2071; Found: 669.2076 $[M + H]^+$.

2.3 | General procedure for the spectroscopic studies

All the spectroscopic measurements were carried out in aqueous CH_3CN medium at room temperature. Stock solutions of ligands L_1 and L_2 (1×10^{-3} M), selected salts of cations (1×10^{-3} M) and anions (1×10^{-4} M) were prepared in CH_3CN/H_2O. Thus, L_1-Al^{3+} and L_2-Al^{3+} solutions for N_3^- detection were prepared by addition of 1.0 equivalent of Al^{3+} to the solution of both L_1 and L_2 (20 μM) in Tris-HCl (10 mM, pH = 7.2) buffer containing CH_3CN/H_2O (7:3, *v/v*) solution. The resulting solution was shaken well before recording the spectra. Each and every fluorescence titration was repeated at least thrice until consistent values were obtained. Jobs continuous variation method was used for determining the binding stoichiometry of the complexation reaction. The association constant (*K*) was calculated from absorbance studies by the linear Benesi–Hildebrand equation.[25] Color changes in solution phase were observed visually under normal light and under a hand-held UV lamp upon addition of various metal ions at room temperature.

3 | RESULTS AND DISCUSSION

3.1 | Synthesis of sensors L_1 and L_2

The synthesis of L_1 and L_2 were prepared in two steps with 92% and 88% overall yields respectively (Scheme 1). The results obtained indicate that, unlike classical heating, MAOS results in higher yields, shorter reaction time, mild reaction condition, simple work-up procedure and better purity offer privilege over other methods where complex chromatographic techniques are required for purification of the target compounds. The structure of sensors were fully characterized by ^{1}H-NMR, ^{13}C-NMR, FT-IR and HRMS spectroscopy and all data are in accordance with the proposed structure. Detailed synthetic process and structure characterization are given in the experimental section and in the Supporting Information.

3.2 | Absorption spectra studies

The metal ion sensing of L_1 and L_2 were first investigated by U*V*-vis absorption spectra. The colorless solutions were very weakly fluorescent and showed no absorption above 450 nm, properties which are characteristic of the predominant ring-closed spirolactam. The predominant spirolactam form was further confirmed by observation of the characteristic carbon resonance near 66 ppm for each of the sensors. The UV-vis spectrum of sensors were recorded in buffer at 25°C and showed an absorption maximum at λ = 315 nm, which may be attributed to the intramolecular π-π* charge transfer transition. On incremental addition of Al^{3+} ions, the absorption intensity at 315 nm increased gradually and a new absorption peak at 565 nm with a shoulder at 525 nm was generated by ring opening with a visual color

change from colorless to pink. The well-defined isosbestic points at 340 and 375 nm clearly indicates the formation of a new complex species between L_1 and Al^{3+} ion (Figure 1). The absorption enhancement is high compared to other metal ions. Selectivity of L_1 was checked in the presence of other metal ions. No significant change in the UV-vis spectrum was observed upon the addition of a 10 equivalent excess of other metal ions of interest: Na^+, K^+, Mg^{2+}, Ca^{2+}, Ni^{2+}, Zn^{2+}, Co^{2+}, Hg^{2+}, Pb^{2+}, Fe^{2+}, Fe^{3+}, Cr^{2+} and Cu^{2+}. Absorption spectra of sensors recorded with the continuous addition of Al^{3+} showed a continuous increase in the absorption at 565 nm and that was employed to calculate binding constants for L_1 and L_2 with Al^{3+} using the Benesi–Hildebrand method. The plot of absorbance of L_1 at 565 nm as a function of mole fraction of added Al^{3+} metal ion reveals that these probes bind to the metal ion in 1:1 stoichiometry (Figure 2). The complex association constant (K) calculated through the Benesi–Hildebrand equation for Al^{3+} with L_1 and L_2 were found to be$3.82 \times 10^4\ M^{-1}$ and $2.41 \times 10^4\ M^{-1}$respectively.

3.3 | Fluorescence spectral response of sensors

To further explore the sensing behavior of L_1 for Al^{3+} ion, the fluorescence spectra of L_1 in CH_3CN with various metal ions were examined. The fluorescence spectra were obtained by excitation at 510 nm, and both the excitation and emission slit were 5 nm. The fluorescence intensity of L_1 upon the additions of metal ions in CH_3CN showed a remarkable sensitivity and selectivity towards Al^{3+}, even though there were relatively small effects with Cu^{2+} and Cr^{3+} (Figure 3a). There was a significant emission intensity enhancement with 1.0 equivalent of Al^{3+} which indicate sensor L_1 is an excellent turn-on sensor for Al^{3+}. This very high fluorescence enhancement is attributed to the formation of ring-open spirolactum in the presence of Al^{3+}. This selectivity for Al^{3+} ions over all other ions is due to selective chelate formation with L_1 to afford an L_1-Al^{3+} complex (Scheme 2). When illuminated with a hand-held UV lamp, the addition of Al^{3+} ions to sensor solution resulted in orange fluorescence emission from L_1 solution (Figure 4 and see also Supporting Information Figure S5). The fluorescence profile of L_2 were very similar to those for sensor L_1: again Al^{3+} registered the highest fluorescence enhancement while other metal ions showed no significant enhancement (Figure 3b). The fluorescence spectrum of sensors L_1 and L_2 showed a peak at 585 nm upon the addition of Al^{3+} corresponding to the delocalization in the xanthenes moiety of rhodamine. It is assumed that the spirolactam form was opened upon the addition of Al^{3+} to sensors and makes a highly delocalized π-conjugated stable complexes with Al^{3+} through their active donor sites (e.g. N and O atoms) of receptor part, though other ions failed which basically indicates that the coordinate moiety of L_1 and L_2 matches perfectly with Al^{3+} ions instead of the other ions. The detection limits of L_1 and L_2 for Al^{3+} ions were estimated based on the fluorescence titration experiment as 32 μM and 47 μM respectively. Furthermore, the effect of pH values on the fluorescence of L_1 and L_2 were also investigated in a pH range from 3 to 10. Figure 5 shows that for free L_1 and L_2 at pH < 5, due to protonation of the open-ring of spirolactam, an obvious color change and fluorescence turn-on appeared. Thus, all the optical measurements were performed in buffer solution with a pH of 7 to keep the sensors in their ring closed form.

3.4 | Detection of azide (N_3^-)

It was interesting to investigate the reversible binding nature of the sensors as shown in Figure 6 and Scheme 2. Due to the high stability of AlN_3, the L_1-Al^{3+} and L_2-Al^{3+} complexes could serve as possible means to detect N_3^-. Figure 6(a) shows the addition of 20 μM of anions N_3^-, CN^-, ClO_4^-, CH_3COO^-, HSO_4^-, $H_2SO_4^{2-}$, SCN^-, Cl^-, I^-, F^-, and OH^- to L_1-Al^{3+} (1:1) of which N_3^- alone quenches the fluorescence, with a slight effect for CN^-, indicating high selectivity for N_3^-. High concentration of CN^- contamination is likely to mislead the fluorescent selectivity of N_3^-. So, when L_1-Al^{3+} is used as the sensor for N_3^-, high concentration of CN^- interference must be eliminated by using mesoporous carbon based adsorbent.[26] The addition of N_3^- to the L_1-Al^{3+} solution led to a change in color of the solutions from pink to colorless, which was observed with the naked eye. The addition of N_3^- to the solution containing L_1-Al^{3+} complex resulted in the reversal of the Al^{3+} induced changes in the emission band at 585 nm in the fluorescence emission spectra. Gradual addition of N_3^- results in continuous decrease in the emission intensity at 585 nm (Figure 6b). Based on fluorescence data, the detection limit of L_1-Al^{3+} for N_3^- was calculated as 12 μM. A similar finding was observed for complex L_2-Al^{3+} towards N_3^- ions (Figure S5). The L_2-Al^{3+} system revealed remarkably selective fluorescence “off” behavior exclusively with N_3^-. The limit of detection value for N_3^- ions was found at 18 μM. Thus, results strongly support that L_1-Al^{3+} and L_2-Al^{3+} binds N_3^- ions with higher selectivity and the process is reversible. The proposed binding mechanism of sensors with Al^{3+} in the presence and absence of azide (N_3^-) is shown in Scheme 2.

3.5 | FT-IR and ^{1}H-NMR study for elucidation of coordination mechanism between sensors and Al^{3+}

To elucidate the coordination mechanism of L_1-Al^{3+} and L_2-Al^{3+} complexes, the FT-IR spectrum of L_1 and L_2 were conducted in the absence and presence of Al^{3+} ion. The characteristic peak of the amide carbonyl $\gamma_{(C=O)}$ shifted from 1680 cm^{-1} to 1614 cm^{-1} in the presence of Al^{3+}, indicating that carbonyl O atoms of the L_1 and L_2 are involved in the coordination of Al^{3+} (Figure S9 and S14). ^{1}H-NMR was also performed by adding Al^{3+} to deuterated dimethyl sulfoxide (DMSO-d_6) solution of L_2 as shown in Figure 7. The **L**$_2$-Al^{3+} complexes were prepared by the additions of 0.25, 0.5 and 1.0 equivalent $AlCl_3{\cdot}6H_2O$ to the DMSO solution of L_2. The peaks observed at δ 10.10 and δ 9.07 are attributable to the phenolic OH and the imine proton (−CH=N−) in L_2. Addition of 1 equivalent of Al^{3+} resulted in the disappearance of the hydroxyl proton indicating the binding of Al^{3+} ion through the phenoxide interaction. Further, the little unfilled-shifts from 9.07 to9.00 ppm and shortening of imine protons were observed because of the complex formation between nitrogen atoms and Al^{3+}. The formation of the L_2-Al^{3+} complex through normal ring opening was confirmed by performing the ^{13}C-NMR experiment with L_2 in the absence and presence of Al^{3+}ions, from which it was observed that the signal at δ = 66 ppm attributable to the tertiary carbon of the spirolactam ring in L_2 was absent from the spectrum of L_2-Al^{3+} complex. Therefore, we propose that the O atom of phenolic OH, N atom of imine and O atom of spiro ring might coordinate to Al^{3+} as shown in Scheme 2.

3.6 | Geometry optimization

To better understand the nature of the coordination of Al^{3+} with sensors, theoretical calculations on structures L_1, L_2, L_1-Al^{3+} and L_2-Al^{3+} were carried out using Spartan'16 software. Density functional theory (DFT), employing the B3LYP functional and the 6–31G* basis set was used to obtain gas phase, optimized geometries of these structures. The optimized structures of L_1, L_2 and their respective Al-complexes are depicted in Figure 8(a) and 8(b). L_1 and L_2 can undergo rotation of *c*. 180° about the N-N bond, producing two prominent cis and trans conformations. For both L_1 and L_2, the trans conformation is more energetically stable than the respective cis one by *c*. 11.3 kJ mol^{-1}, owing to anti arrangement of the methoxy (−OMe) group and the xanthene moiety in trans L_1 and to the anti arrangement of the hydroxyl (−OH) group and the xanthene moiety in trans L_2. Additionally, in trans L_1 the energy gap between the highest occupied molecular orbital (HOMO) (−4.81 eV) and the lowest unoccupied molecular orbital (LUMO) (−1.34 eV) is 3.47 eV, and in cis L_1 the gap, HOMO (−5.03 eV) and LUMO (−1.35 eV), is3.68 eV. In trans L_2, the energy gap, HOMO (−4.86 eV) and LUMO (−1.29 eV) is 3.57 eV, and in cis L_2 the energy gap, HOMO (−5.05 eV) and LUMO (−1.22 eV) is 3.83 eV, suggesting that trans L_1 and trans L_2 are the major equilibrium conformations available stereochemically for direct Al^{3+} coordination. Also, in trans L_1, the electron density is delocalized over the entire xanthene moiety with some found on the spirolactam ring as well as on the imine and the ortho-methoxy naphthalene moieties (Figure 8a). In cis L_1, the electron density is mainly localized on half of the xanthene moiety (Figure S15). In both trans L_2 and cis L_2, the electron density is mainly located over the entire xanthene moiety with some found on the lactam ring nitrogen of both. Moreover, some electron density is also found on the carbonyl oxygen in trans L_2 but not on the carbonyl oxygen in cis L_2 (Figure 8b and Figure S15).

Density functional calculations of molecular interactions of *trans*-L_1 and *trans*-L_2 with aqueous aluminum (Al^{3+}) nitrate solution revealed that both sensors are energetically stabilized on binding with Al^{3+} ions. For instance, upon formation of L_1-Al^{3+} salt complex, the HOMO-LUMO energy gap in *trans*-L_1 (ΔE = 3.47 eV) decreased to ΔE = 2.40 eV, and upon formation of L_2-Al^{3+} complex, the HOMO-LUMO energy gap in *trans*-L_2 (ΔE = 3.57 eV) decreased to 2.22 eV. In L_1-Al^{3+} salt complex, formulated as [Al (L_1) $NO_3)_2(H_2O)_2$] [NO_3], HOMO is primarily delocalized over the methoxy naphthalene moiety, while LUMO is primarily delocalized over the xanthene moiety. In L_2-Al^{3+} complex, formulated as Al (L_2) $(NO_3)_2(H_2O)$, HOMO is found over the tricyclic structure about Al^{3+} while LUMO is delocalized over the xanthene moiety (Figure 8a and 8b).

Vertical electronic excitations of optimized B3LYP/6–31G* *trans*-L_1, *trans*-L_2 and their respective complexes were computed using time-dependent-density functional theory (TD-DFT) Spartan'16 software calculations, formalized in water and using a conductor-like polarizable continuum model (CPCM). In the TD-DFT UV-vis spectrum of *trans*-L_1, an absorption band at λ = 379.24 nm with a vertical excitation energy of 3.2693 eV and corresponding to HOMO-2 → LUMO excitation (oscillator strength = 0.4632) dominates as shown in Table S5. While in the TD-DFT UV-vis spectrum of *trans*-L_1-Al^{3+} salt complex, an absorption band at λ = 422.57 nm dominates, corresponding to HOMO→ LUMO excitation (vertical excitation energy = 2.9341 eV and oscillator strength = 1.0951), (Table S6). In the

case of trans-L_2, an absorption band at λ = 344.32 nm dominates, corresponding to HOMO-2 → LUMO excitation with a vertical excitation energy of 3.6008 eV and an oscillator strength = 0.3152 as shown in Table S8. For *trans*-L_2-Al^{3+} complex, an absorption band at λ = 456.19 nm dominates, corresponding to HOMO-1 → LUMO and HOMO→LUMO excitations with a vertical excitation energy of 2.7178 eV and an oscillator strength = 0.7824 (Table S9). The detailed theoretical studies, including the TD-DFT calculations (Tables S1–S9), are in good agreement with the experimental observation.

4 | CONCLUSION

We have developed reversible fluorescent sensors L_1 and L_2 for the selective and sensitive sequential detections of Al^{3+} and N_3^- via the fluorescence spectral changes. Upon binding to Al^{3+}, obvious detectable change in fluorescence was observed due to the CHEF effect. The *in situ* prepared L_1-Al^{3+} and L_2-Al^{3+} complexes were used to detect N_3^- via the metal-displacement approach which displayed an excellent selectivity and sensitivity towards N_3^-. Thus, upon the addition of N_3^- to complexes, the intensity of the 585 nm band decreases, suggesting release of L_1 and L_2 from the aluminum complexes. Stoichiometry and binding mechanisms for both sensors are well characterized and established by the respective spectroscopic techniques. These results clearly demonstrate that our proposed sensors could be useful for the analysis of Al^{3+} and N_3^- in environmental samples and even for biological studies.

Supplementary Material

Refer to Web version on PubMed Central for supplementary material.

ACKNOWLEDGEMENTS

The authors acknowledged Morgan State University and the Institute of General Medical Science of the National Institute of Health (Grant No. UL1GM118973) for financial support.

Funding information

Institute of General Medical Science of the NIH, Grant/Award Number: UL1GM118973

REFERENCES

[1]. Xu Y, Mao S, Peng H, Wang F, Zhang H, Opeyemi A, Wu H, JOL 2017, 192, 56.

[2]. Perl D, Gajdusek D, Garruto R, Yanagihara R, Gibbs C, Science 1982, 217, 1053. [PubMed: 7112111]

[3]. Tang J, Li C, Li Y, Lu X, Qj H, Anal. Chim. Acta 2015, 888, 155. [PubMed: 26320971]

[4]. Zhan T, Feng X, Tong B, Shi J, Chen L, Zhi J, Dong Y, Chem. Commun 2012, 48, 416.

[5]. Alvarez E, Fernandez M, Monterrooso C, For. Ecol. Manage 2005, 211, 227.

[6]. Upadhyay K, Kumar A, Org. Biomol. Chem 2010, 8, 4892. [PubMed: 20820652]

[7]. Zhao Y, Lin Z, Liao H, Duan C, Meng Q, Inorg. Chem. Commun 2006, 9, 966.

[8]. Sahana A, Banerjee A, Guha S, Lohar S, Chattopadhyay A, Mukhoppadhyay S, Das D, Analyst 2012, 137, 1544. [PubMed: 22328988]

[9]. Lohar S, Banerjee A, Sahana A, Banik A, Mukhopadhyay S, Das D, Anal. Methods 2013, 5, 442.

[10]. Morita T, Perrella MA, Lee ME, Kourembanas S, Proc. Natl. Acad. Sci 1995, 92, 1475. [PubMed: 7878003]

[11]. Jeong J, Rao B, Son Y, Sens. Actuators B 2015, 208, 75.
[12]. Gunnlaugsson T, Glynn M, Tocii GM, Kruger PE, Coord. Chem. Rev 2006, 250, 3094.
[13]. Weerasinghe AJ, Abebe F, Venter A, Sinn E, J. Fluoresc 2016, 26, 891. [PubMed: 26994908]
[14]. Weerasinghe AJ, Abebe F, Sinn E, Tetrahedron Lett. 2011, 52, 5648.
[15]. Wang HH, Xue L, Yu LL, Qian YY, Jiang H, Dyes Pigm. 2009, 91, 350.
[16]. Hue F, Su J, Sun Y, Yin C, Tong H, Nie Z, Dyes Pigm. 2010, 86, 50.
[17]. Li S, Zhang D, Wang M, Ma S, Liu J, Zhao Y, Ye Y, J. Fluoresc 2016, 26, 769. [PubMed: 26781110]
[18]. Wei Y, Aydin Y, Zhang Y, Liu Z, Guo M, Chem. Bio. Chem 2012, 13, 1569.
[19]. Sikdar A, Panja S, Biswas P, J. Fluoresc 2012, 22, 443. [PubMed: 21938389]
[20]. Huang J, Xu Y, Qian X, J. Org. Chem 2009, 74, 2167. [PubMed: 19209877]
[21]. Huang W, Zhou P, Yan W, He C, Xiong L, Li F, Duan C, J. Environ. Monit 2009, 11, 330. [PubMed: 19212590]
[22]. Sarkar M, Banthia S, Samanta A, Tetrahedron Lett. 2009, 47, 7575.
[23]. Weerasinghe AJ, Schmiesing C, Sinn E, Tetrahedron Lett. 2009, 50, 6407.
[24]. Xiang Y, Tong A, Jin P, Ju Y, Org. Lett 2006, 8, 2863. [PubMed: 16774276]
[25]. Abebe F, Sinn E, Tetrahedron Lett. 2011, 52, 5234.
[26]. Lee E, Lee S, Heo N, Stucky G, Jun Y, Hong W, Chem. Commun 2012, 48, 3942.

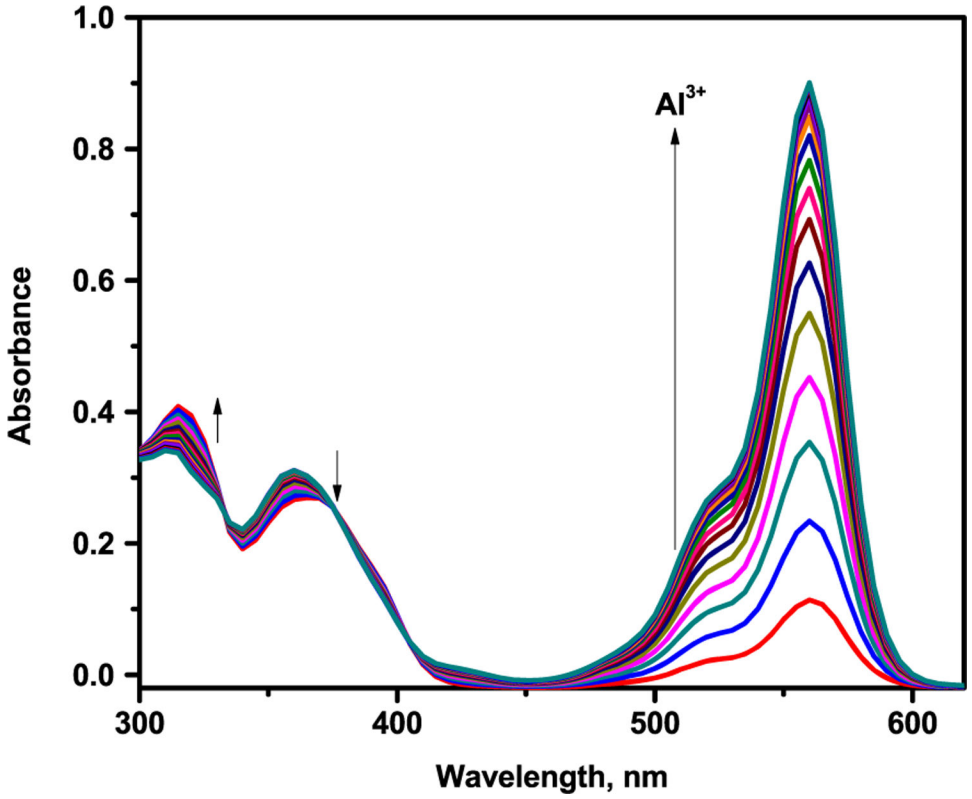

FIGURE 1.
UV-vis spectra of L_1 (10 μM) with Al^{3+} (0–23 μM) in CH_3CN/H_2O (7:3 *v/v*) solution

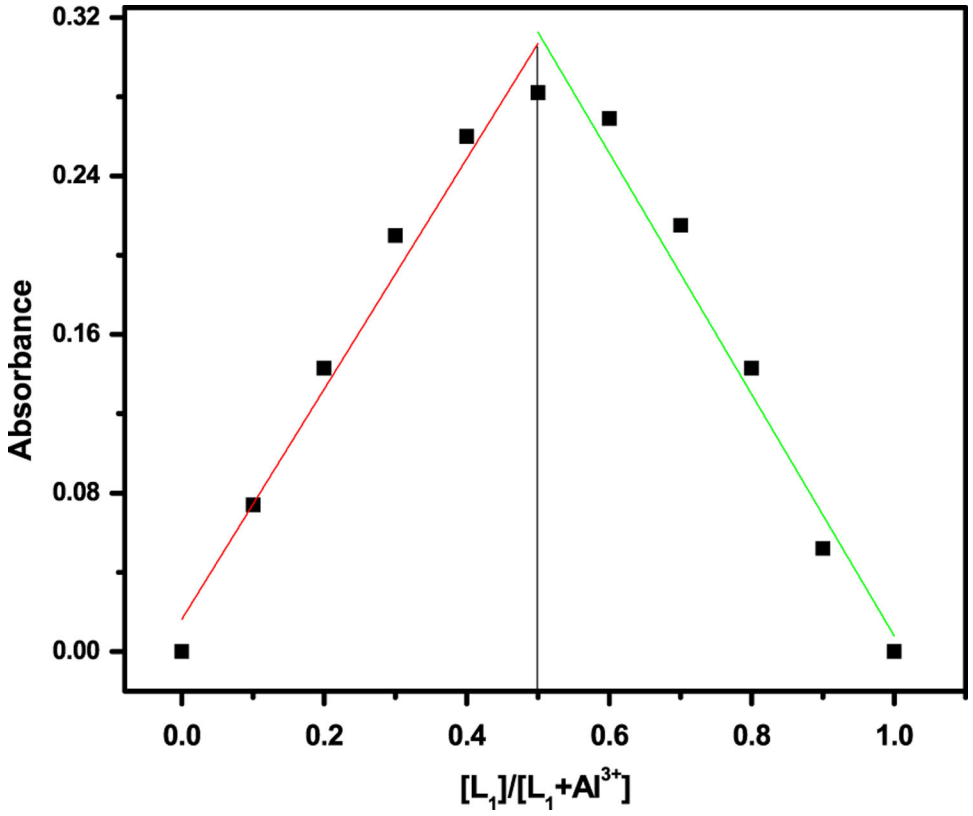

FIGURE 2.

Absorbance Job's plot for determination of L_1-Al^{3+} complex (10 μM) in CH_3CN/H_2O (7:3 *v/v*) solution

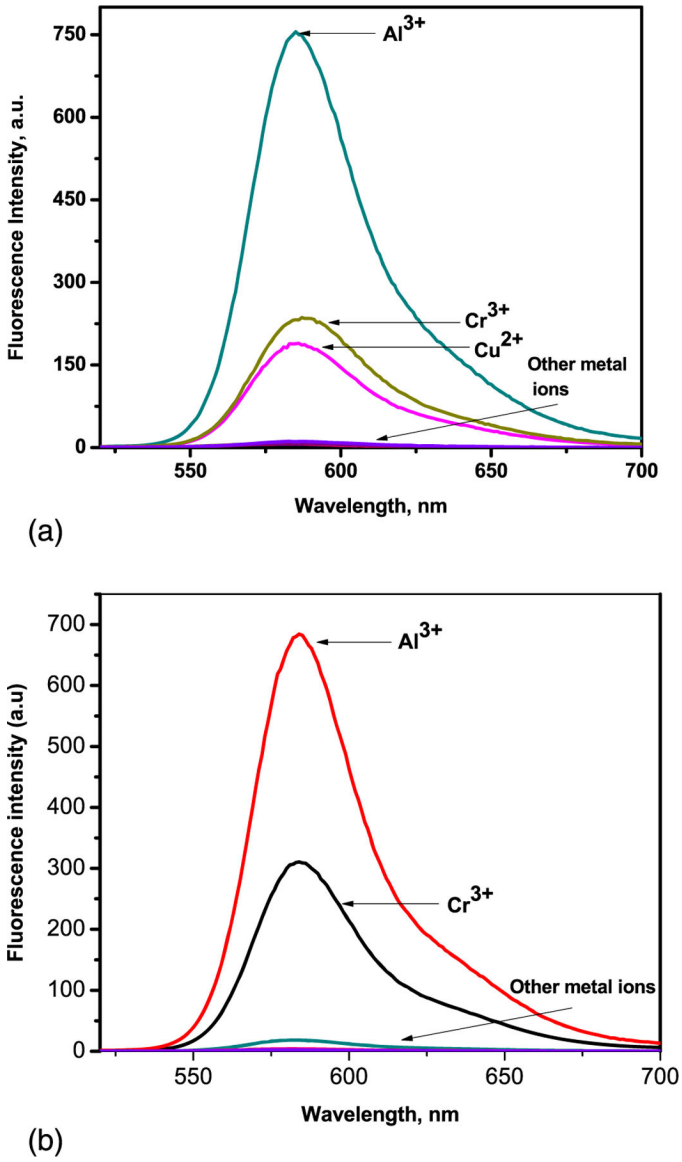

FIGURE 3.

(a) Fluorescence spectra of L_1 (10 μM) with metal ions (10 μM) in CH_3CN/H_2O (7:3 *v/v*) solution (λ_{ex} = 510 nm). (b) Fluorescence spectra of L_2 (10 μM) with metal ions (10 μM) in CH_3CN/H_2O (7:3 *v/v*) solution (λ_{ex} = 510 nm)

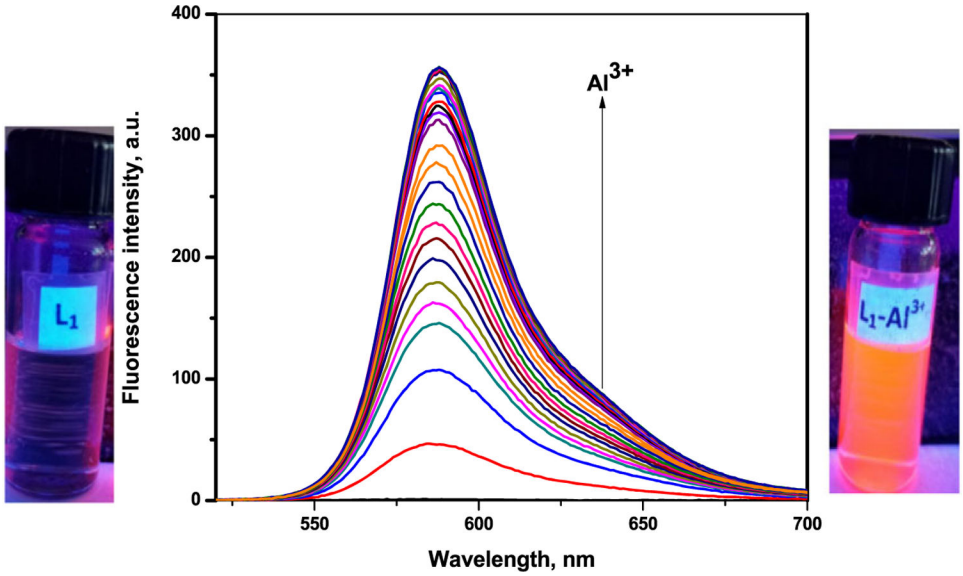

FIGURE 4.

Fluorescence spectral titration of L_1 (10 μM) on the incremental addition of $Al(NO_3)_3$ (23 equivalents) (λ_{ex} = 510 nm)

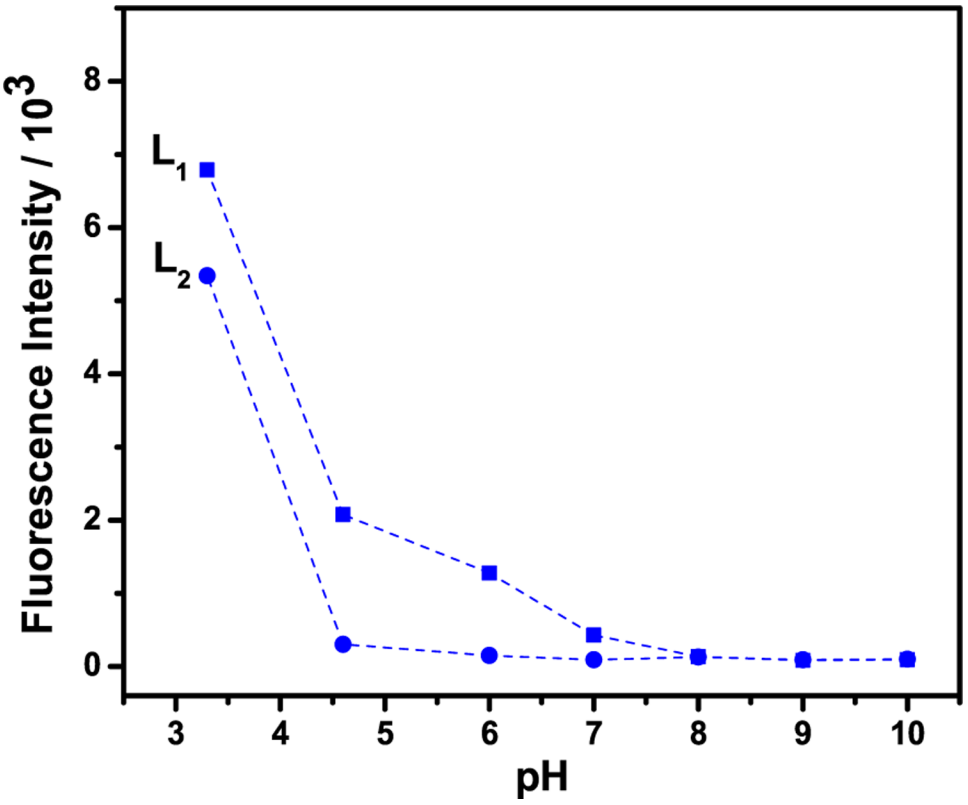

FIGURE 5.
Effect of pH values on fluorescence intensity of sensors L_1 and L_2 (10 μM)

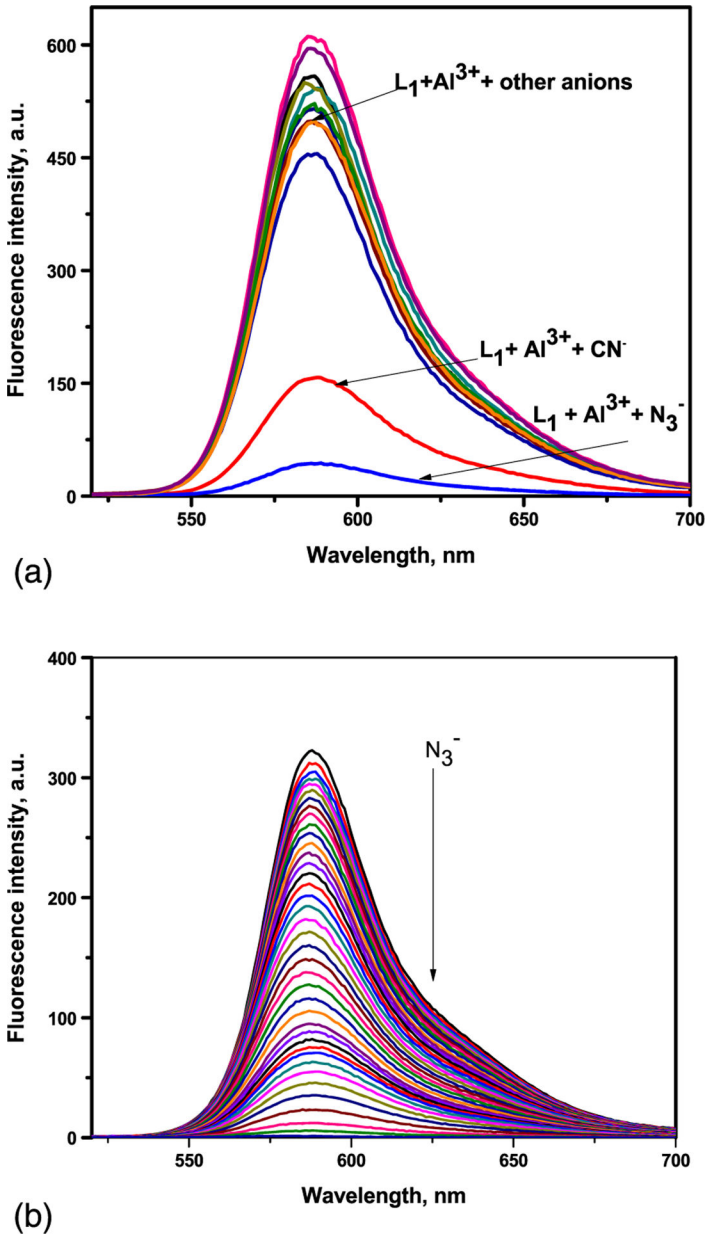

FIGURE 6.

(a) Fluorescence spectra of L_1-Al^{3+} (1:1) with anions (10 μM) (λ_{ex} = 510 nm). (b) Fluorescence spectral titration of L_1-Al^{3+} (23 equivalents of Al^{3+}) on the incremental addition of N_3^- (up to35 equivalents) (λ_{ex} = 510 nm)

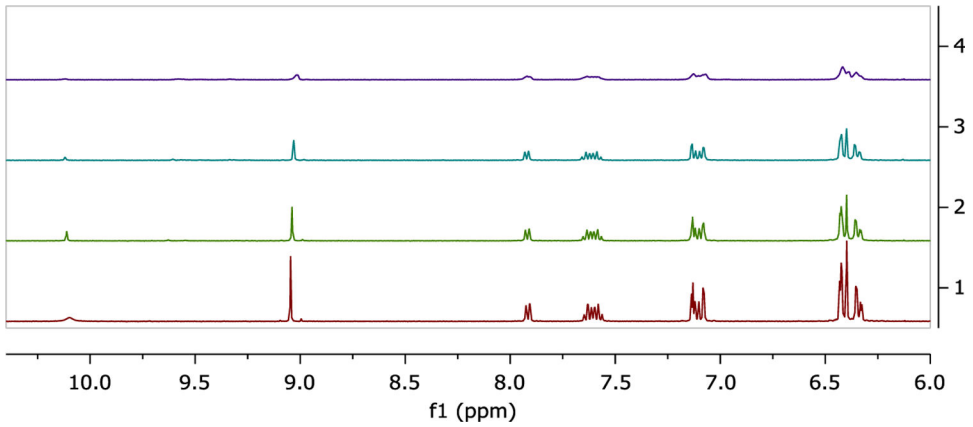

FIGURE 7.

^{1}H-NMR spectral changes of L_2 (8 mM) in DMSO-d_6 and titrated with 0–1.0 equivalents of Al^{3+} in deuterated water

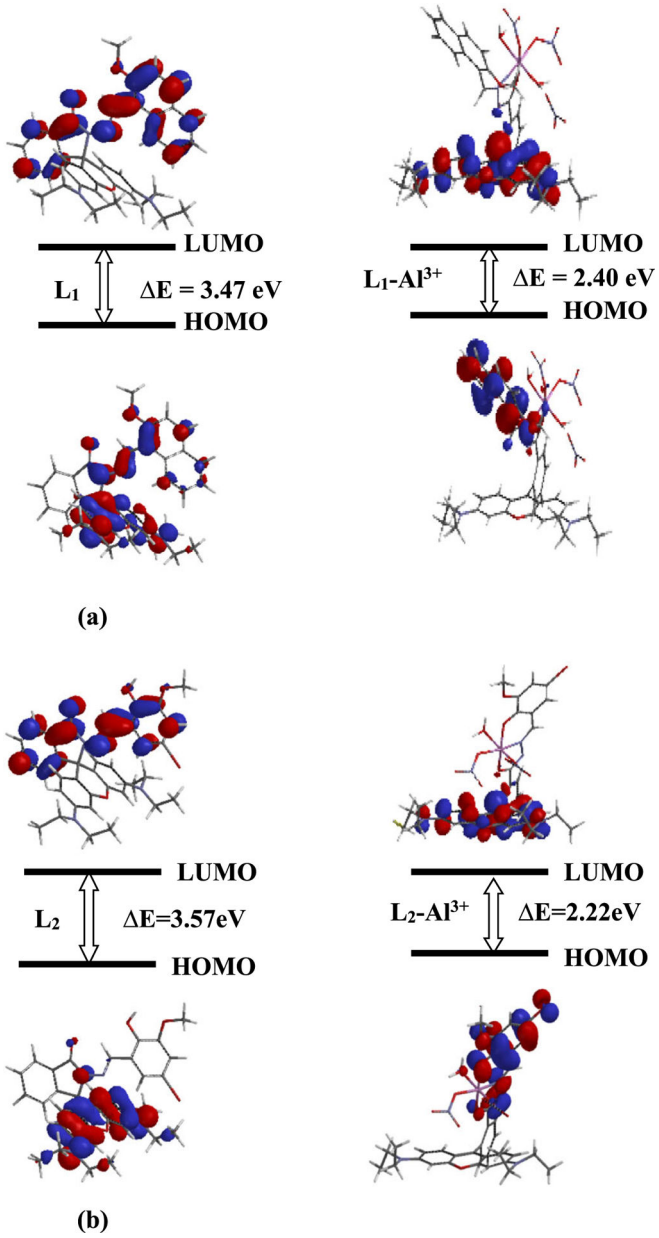

FIGURE 8.

(a) The optimized structures and energy correlation of the HOMO-LUMO gap between L_1 and L_1-Al^{3+} salt. (b) The optimized structures and energy correlation of the HOMO-LUMO gap between L_2 and L_2-Al^{3+} complex

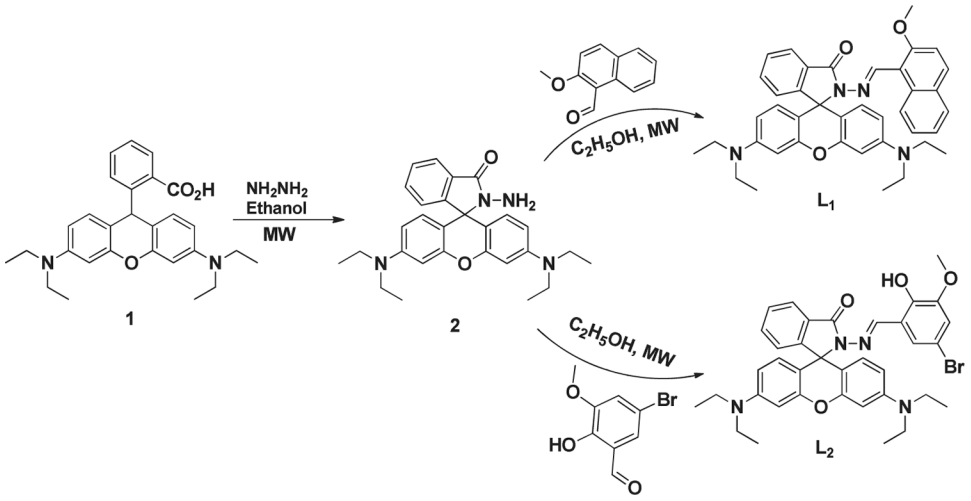

SCHEME 1.
Chemical structure and synthetic route of L_1 and L_2

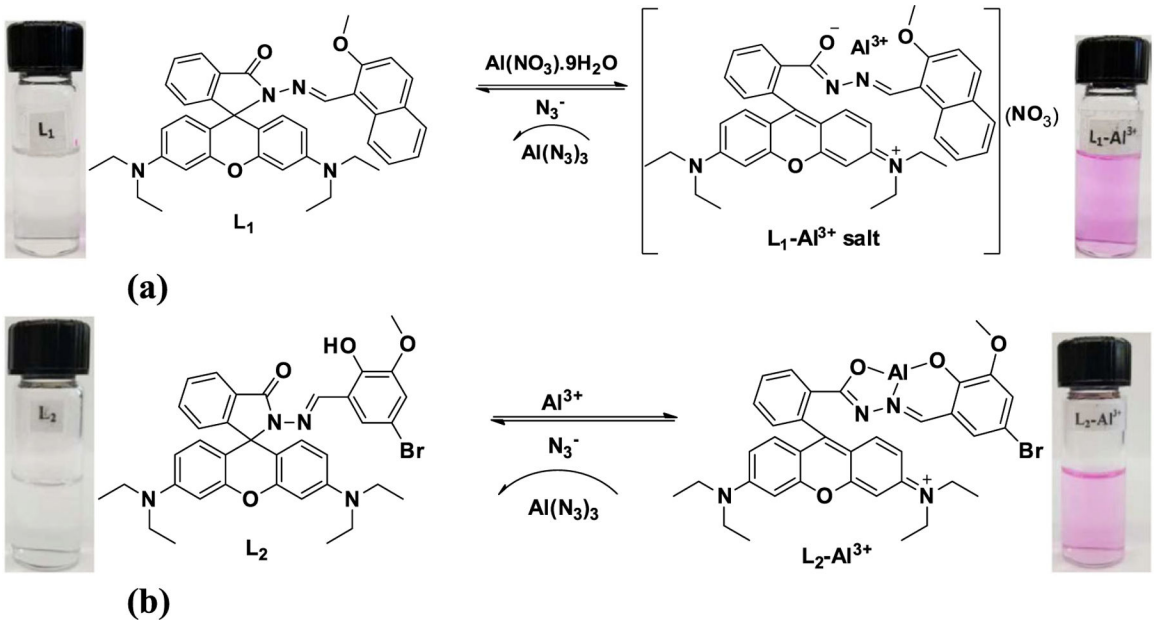

SCHEME 2.

A possible proposed binding mechanism of sensor L_1 (a) and L_2 (b) towards Al^{3+} in the presence and absence of azide (N_3^-)